# INFLUENCE OF PREVIOUS OPERATIONAL CYCLE ON THE MICROSTRUCTURE OF REJUVENATED NI-BASE SUPERALLOY GAS TURBINE BLADES AFTER THEIR RETURN TO SERVICE


**by**

**Evgenia Lvov**

**Senior Metallurgist**

**and**

**Donald Norsworthy**

**Manager of Technical Services**

**Preco Turbine & Compressor Services, Inc.**

**Houston, Texas**


*Evgenia Lvov is a Senior Metallurgist in the Metallurgical Laboratory at Preco Turbine & Compressor Services, Inc., Houston, Texas. She is responsible for performing metallurgical analysis of turbine and compressor parts submitted to Preco for repair and refurbishment, advising on rejuvenating procedures, and conducting quality control. Before emigrating to the USA in 1992, Dr. Lvov was a Senior Scientist in the Department of Physical Metallurgy at the Ural Polytechnic University, Ekaterinburg, Russia, working on the projects concerning high-strength structural steels, titanium alloys, and heat-resistant alloys. She is using her expertise in physical metallurgy to ensure that Preco's Metallurgical Laboratory is on the leading edge of repair technology.*

*Dr. Evgenia Lvov earned her M.S. (Physics of Metals) and Ph. D. (Physical Metallurgy) degrees at the Ural Polytechnic University, Ekaterinburg, Russia. She is a member of ASM International and has authored several publications in the field of physical metallurgy.*

*Donald Norsworthy is the Manager of Technical Services at Preco Turbine & Compressor Services, Inc., in Houston, Texas. He is responsible for the Metallurgical Laboratory, Inspection and Testing Services, Welding Engineering and Advanced Process Development, Heat Treating, and Coating and Stripping Processes. His previous experience includes metallurgy and welding engineering for GE Power Generation, GE Aircraft Engines, Teledyne Continental Aircraft Engines, TVA Nuclear Construction, and Westinghouse Industrial Equipment.*

*Mr. Norsworthy earned his B.S. degree (Material Engineering, 1976) at the University of South Florida. He was chairman of the ASM Gulf Coast Chapter in 1987 and 1988, and he is also a long-standing member of AWS.*


## ABSTRACT

The practice of rejuvenating reheat treatments, with and without hot isostatic pressing (HIP), has been successful in restoring severely overaged gas turbine blade microstructure and alloy properties to a nearly "as-new" condition. There are numerous studies on service-induced microstructural damage and rejuvenating techniques of the Ni-base superalloys used in turbomachinery. However, data are scarce on alloy behavior after the rejuvenated blade is returned to service. The presented study concerns specific irreversible service-induced microstructural changes that can alter the aging kinetics of rejuvenated superalloy blades in the next service cycle. It was found that advanced decomposition of primary MC carbides during previous service and the consequent changes of the γ-matrix chemical composition, which occur when the blades undergo the rejuvenating heat treatment, can cause a considerable acceleration of the aging process upon their return to service for the next operational period.


## INTRODUCTION

Gas turbine blades made from Ni-base superalloys experience the effect of high temperatures and stresses during service, which inevitably cause various microstructural changes. The microstructure deterioration can lead to a degradation of mechanical properties, such as tensile strength and creep resistance.

The microstructure of cast Ni-base superalloys consists of the following phases:

- *Austenitic γ-matrix*—Face-centered cubic Ni-base phase with high percentage of solid-solution strengthening elements such as cobalt (Co), iron (Fe), chromium (Cr), molybdenum (Mo), and tungsten (W)
- *γ'-phase ($Ni_3Al$, Ti)*—Precipitated in γ-matrix; this phase is the principal strengthening constituent responsible for high creep resistance
- *Primary MC carbides*—Form during solidification (M stands for metal and can be titanium (Ti), tantalum (Ta), niobium (Nb), or hafnium (Hf), depending on the alloy composition); they are distributed heterogeneously through the alloy, both on the grain boundaries and inside the grains and are usually bulky irregularly shaped particles
- *Secondary $M_{23}C_6$ carbides* (M is predominantly Cr, but it can be replaced in part with nickel (Ni), Mo, and W)—Form on the grain boundaries as a chain of fine globular particles and as such serve to increase creep strength by preventing the grains from sliding

Extensive studies have shown that prolonged thermal and stress exposure causes overaging of the alloy microstructure, that is, γ'-phase coarsening and coalescence, formation of continuous secondary $M_{23}C_6$ carbide films on the grain boundaries, primary MC carbide degeneration, and σ-phase formation, which have detrimental effect on creep resistant properties (Stevens and Flewitt, 1978; Stevens and Flewitt, 1979a; Ross and Sims, 1984; Castillo and Koul, 1986; Koul and Castillo, 1994; Tawancy, et

al., 1994; Xuebing, et al., 1998; Daleo and Wilson, 1998). Most of these changes are reversible, and numerous studies have demonstrated the possibility of the restoration of the blade microstructure and properties after service. The implementation of the rejuvenating procedures, such as an appropriate heat treatment and hot isostatic pressing (HIP) have proven to be able to restore even severely overaged microstructure and alloy properties to a practically "as-new" condition, and they are currently employed successfully throughout the industry (Stevens and Flewitt, 1979b; Beddoes and Walace, 1980; Floyd, et al., 1983; Koul and Castillo, 1988; Maccagno, et al., 1989; Baldan, 1995; Hakl, et al., 1995). However, some service-induced microstructural changes, such as primary MC carbide decomposition, are irreversible, and might affect the aging process after rejuvenated blades are returned to service. Published data are scarce on the behavior of rejuvenated blades during the next service cycle. The presented study concerns this problem and will discuss the influence of the previous microstructural degradation on the aging kinetics of rejuvenated gas turbine blades made from Ni-base superalloys IN-738 and GTD-111.

## EXPERIMENTAL PROCEDURES

*Materials and Treatments*

Four service-exposed blades from four different gas turbines with different service histories were chosen for this study. They will be further referenced as Blade 1, Blade 2, Blade 3, and Blade 4.

- Blade 1—First-stage blade from GE MS7001EA turbine, conventionally cast (CC) alloy GTD-111.
- Blade 2—Second-stage blade from GE MS7001B turbine, IN-738 alloy.
- Blade 3—Second-stage blade from GE MS7001B turbine, IN-738 alloy.
- Blade 4—Second-stage blade from GE MS7001E turbine, IN-738 alloy.

The elemental analyses of these blades (except carbon) were performed using an atomic absorption spectrophotometer. Carbon contents were analyzed using a combustion thermal conductivity method. The chemical compositions of the analyzed alloys are given in Table 1.

*Table 1. Chemical Compositions of the Studied Blades.*

| Element | Element content, wt. % | | | |
|---|---|---|---|---|
| | Blade 1 (GTD-111) | Blade 2 (IN-738) | Blade 3 (IN-738) | Blade 4 (IN-738) |
| Carbon | 0.095 | 0.097 | 0.089 | 0.110 |
| Chromium | 13.78 | 15.36 | 16.07 | 16.39 |
| Cobalt | 9.52 | 8.32 | 8.52 | 8.35 |
| Aluminum | 2.90 | 3.48 | 3.56 | 3.63 |
| Titanium | 4.75 | 3.31 | 3.25 | 3.18 |
| Molybdenum | 1.60 | 1.86 | 1.84 | 1.79 |
| Tungsten | 3.86 | 2.65 | 2.71 | 2.73 |
| Niobium | - | 1.22 | 1.15 | 1.07 |
| Tantalum | 2.92 | 1.20 | 1.42 | 1.39 |
| Iron | - | 0.36 | 0.29 | 0.19 |
| Boron | 0.014 | 0.008 | 0.013 | 0.014 |
| Silicon | 0.019 | 0.015 | 0.013 | 0.009 |
| Nickel | Balance | Balance | Balance | Balance |

The blades were sectioned by the wire electrical discharge machining (EDM) process at two locations: the shank and the airfoil at approximately one-half airfoil height. The metallographic specimens were cut from the shank dovetail and from the leading edge at one-half airfoil height; the specimens for stress-rupture tests were cut from the shank and from the mid-airfoil section (Figure 1). The blade shank metal served as an indicator of the initial metal condition, since the service temperature of the shank is relatively low and does not cause a degradation of the metal microstructure during service. The maximum service-induced damage of the blade material from a combination of high temperature and operating stresses occurs in the middle of the airfoil (pitch line). The comparison of the microstructure of the blade shank and mid-airfoil served to assess service-related changes. One set of the specimens was cut from each blade in its as-received condition. The blades then underwent the rejuvenation, consisting of HIP and heat treatment specific for the alloy, after which the second set of specimens was cut. The rejuvenating procedures for the studied alloys were:

- CC GTD-111:
  - HIP at 2200°F at 15 ksi of argon, for four hours, furnace cool
  - 2175°F for two hours in vacuum, cool to 2000°F within 10 minutes
  - 2000°F for two hours in vacuum, argon quench
  - 1925°F for two hours in vacuum, argon quench
  - 1550°F for 16 hours in vacuum, argon quench
- IN-738:
  - HIP at 2175°F at 15 ksi of argon, for four hours, furnace cool
  - 2175°F for two hours in vacuum, cool to 2050°F within 10 minutes
  - 2050°F for four hours in vacuum, argon quench
  - 1550°F for 16 hours in vacuum, argon quench

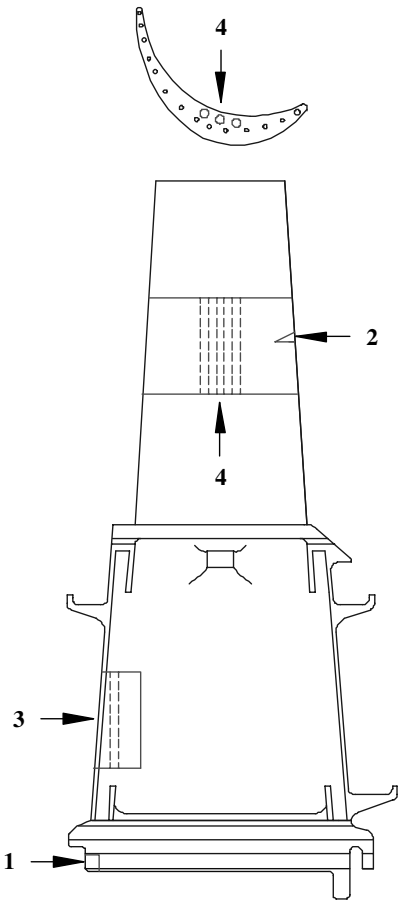


*Figure 1. Blade Section Plan. ((1) Metallographic shank specimen; (2) Metallographic leading edge specimen; (5, 6) Cylinder bars for stress-rupture test specimens.)*

In order to study the aging kinetics after the rejuvenation, the blades were aged at 1550°F for 1000 hr; interruptions of the aging were made after 200 hr and 500 hr in order to cut the specimens. The temperature of 1550°F was chosen because it falls in the region of the maximum secondary carbide precipitation for the studied alloys.

*Experimental Techniques*

The examination of the blade microstructure was performed using optical and scanning electron microscopy (SEM). Secondary electron imaging (SEI) and backscattered electron imaging (BEI) were used to observe etched and as-polished surfaces. The specimens were etched electrolytically with 10 percent water solution of chromic acid ($Cr_2O_3$) or chemically with Kalling's reagent (5 g $CuCl_2$ + 3 mL $HNO_3$ + 50 mL ethanol). Energy-dispersive spectroscopy (EDS) system with thin window light element detector was used to determine the elemental distribution of various phases.

The microhardness of the γ-matrix (with precipitated γ′-phase particles) of the metallographic specimens was measured in order to evaluate the degree of the γ-matrix solid-solution and precipitation-strengthening effect, which correlates with the degree of the alloy overaging.

Stress-rupture tests were performed according to ASTM E139 (1996). The test conditions were chosen based on the creep-rupture curves given in *Aerospace Structural Metals Handbook* (1997), *Heat-Resistant Materials* (1997), and *Atlas of Creep and Stress-Rupture Curves* (1998), with a purpose to conduct a test within a reasonable time (approximately 100 hr) at a temperature close to the service temperature: 1500°F at 70 ksi for CC GTD-111 alloy; 1500°F at 65 ksi for IN-738 alloy. Short-term 24-hour stress-rupture tests at 1450°F at 85 ksi for CC GTD-111 and 1400°F at 85 ksi for IN-738 alloy were also performed. Fracture surfaces of several specimens were examined using SEM.

## RESULTS AND DISCUSSION

*The Blades in the As-Received Condition*

The microstructure of the shank specimens of Blade 1 and Blade 2 is presented in Figure 2 and Figure 3, respectively (the microstructure of the Blade 3 and Blade 4 shank specimens is very similar to that of Blade 2). The shank microstructure is typical for a virgin cast superalloy: γ′-phase exists in three distinctive morphologies—eutectic lamellar γ′ formed between dendrite arms, primary cuboidal γ′ (average side size 0.7 μm in GTD-111 and 0.4 μm in IN-738), and very fine secondary spheroidal γ′; primary MC carbides formed at the grain boundaries and in the interdendritic areas; fine globular secondary $M_{23}C_6$ carbides decorated the grain boundaries.

The micrographs of the Blade 1 and Blade 2 leading edge specimens at one-half airfoil height are presented in Figure 4 and Figure 5, respectively (the microstructure of the Blade 3 and Blade 4 leading edge specimens is very similar to that of Blade 2). Service-induced changes in the leading edge microstructure compared to that of the shank are significant and typical for service-exposed gas turbine blades. The micrographs revealed severe overaging induced by thermal and stress exposure during service. The cuboidal primary γ′ precipitates rounded and coarsened considerably at the expense of the secondary γ′, their diameter ranges from 0.8 μm to 1.5 μm in GTD-111 and from 0.6 μm to 1.3 μm in IN-738. The grain-boundary $M_{23}C_6$ carbide particles coarsened and coalesced, overloading the grain boundaries and forming continuous films at some areas; primary MC carbides degenerated losing their sharp edges.

The service-induced deterioration of the airfoil microstructure caused a significant reduction of the stress-rupture life, ductility, and microhardness compared to that of the shank. Excessive grain-boundary $M_{23}C_6$ carbide precipitation led to decreasing creep resistance; coarsening and coalescence of γ′ precipitates caused a decrease of the tensile strength. The reduced microhardness of the airfoil specimens indicates the overall decrease of solid-solution and precipitation-hardening effects in the γ-matrix of the airfoil

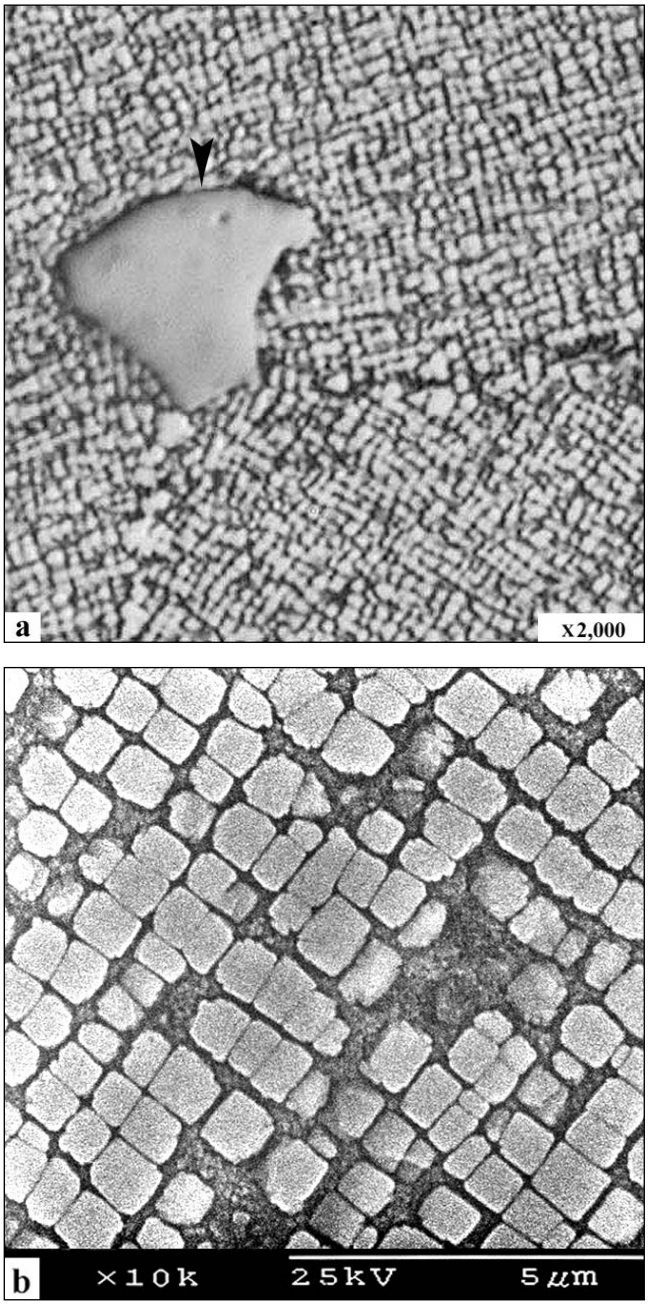


*Figure 2. Microstructure of Blade 1 Shank Specimen in the As-Received Condition. ((a) Optical micrograph; (b) SEM micrograph. Arrowhead indicates primary MC carbide. (Etchant–electrolytic chromic acid))*

midsection as a result of the service-induced overaging. The results of the stress-rupture and microhardness tests are presented in Table 2 and Table 3, respectively.

*Table 2. Stress-Rupture Test Results of the Blades in the As-Received Condition.*

| Specimen location | Blade 1 | | Blade 2 | | Blade 3 | | Blade 4 | |
|---|---|---|---|---|---|---|---|---|
| | Shank | Airfoil | Shank | Airfoil | Shank | Airfoil | Shank | Airfoil |
| Test conditions | 1500°F @ 70 ksi | | 1500°F @ 65 ksi | | 1500°F @ 65 ksi | | 1500°F @ 65 ksi | |
| Time to fracture, hr | 113.4 | 15.1 | 83.8 | 20.9 | 74.1 | 21.3 | 81.2 | 31.4 |
| Elongation, % | 6.9 | 4.4 | 6.5 | 4.9 | 7.9 | 4.3 | 6.7 | 4.4 |
| Reduction in area, % | 11.6 | 4.8 | 9.6 | 6.7 | 12.1 | 6.4 | 9.9 | 6.0 |

*Table 3. Microhardness of the Blades in the As-Received Condition.*

| MICROHARDNESS $H_V$ | | | | | | | |
|---|---|---|---|---|---|---|---|
| **Blade 1** | | **Blade 2** | | **Blade 3** | | **Blade 4** | |
| Shank | Leading edge | Shank | Leading edge | Shank | Leading edge | Shank | Leading edge |
| 429 | 362 | 427 | 354 | 413 | 348 | 392 | 359 |

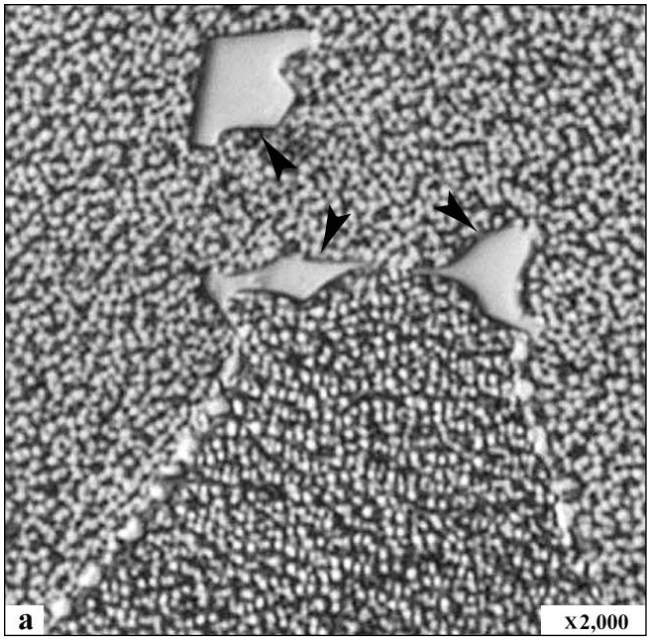


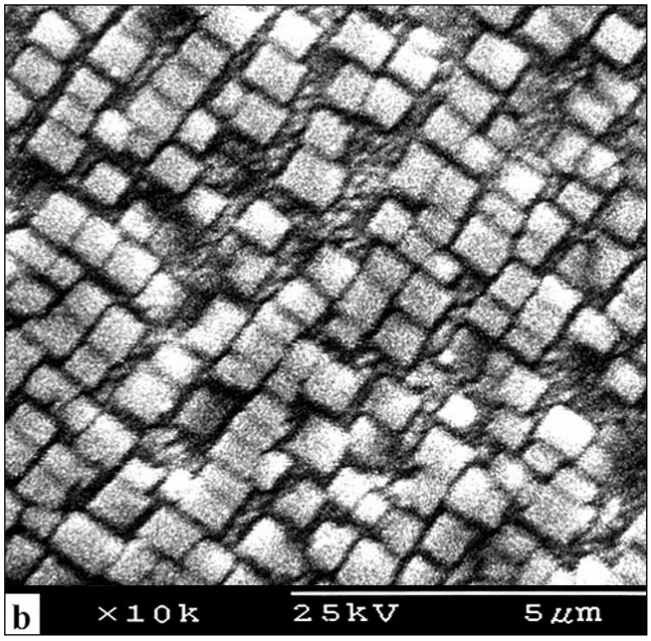


*Figure 3. Microstructure of Blade 2 Shank Specimen in the As-Received Condition. ((a) Optical micrograph; (b) SEM micrograph. Arrowheads indicate primary MC carbide. (Etchant–electrolytic chromic acid))*

Special attention was given to a study of the primary MC carbide decomposition, due to the fact that it is an irreversible process and can affect the behavior of a rejuvenated alloy during subsequent service, as well as to the fact that the data on this subject are insufficient. The SEM micrographs of the degenerated MC carbides and energy-dispersive X-ray spectra are presented in Figures 6, 7, 8, and 9. It can be noted that MC decomposition results in a considerable reduction of its size and a formation of numerous $M_{23}C_6$ carbides at the edges of the original MC carbides. $M_{23}C_6$ carbides formed also in the lathlike morphology at the MC periphery as well as in the grain interiors, which was confirmed by EDS analyses. The diminished core of the degenerated MC carbide is surrounded by a smooth-looking substance being a product of MC decomposition along with $M_{23}C_6$ carbides (Figures 6 and 7). EDS analyses revealed the composition of the primary MC carbides as (Ti, Ta, Mo, Ni, Cr)C in GTD-111 alloy and (Ti, Ta, Nb, Mo, Ni, Cr)C in IN-738 alloy (Figures 8 and 9). The replacement of the strong carbide forming atoms such as Ti, Ta, and Nb, with Mo, Ni, and Cr atoms, is known to weaken the interatomic bonds in the MC carbides resulting in a decrease of their stability. This leads to the MC decomposition with a formation of more stable $M_{23}C_6$-type carbides.

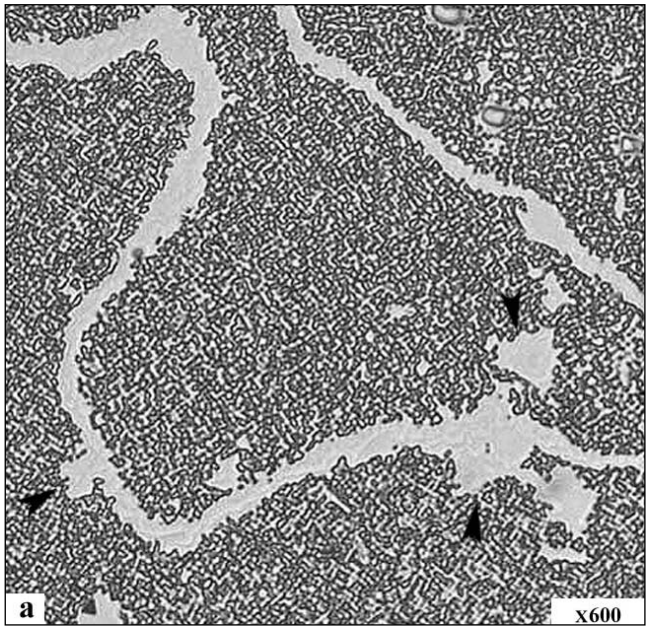


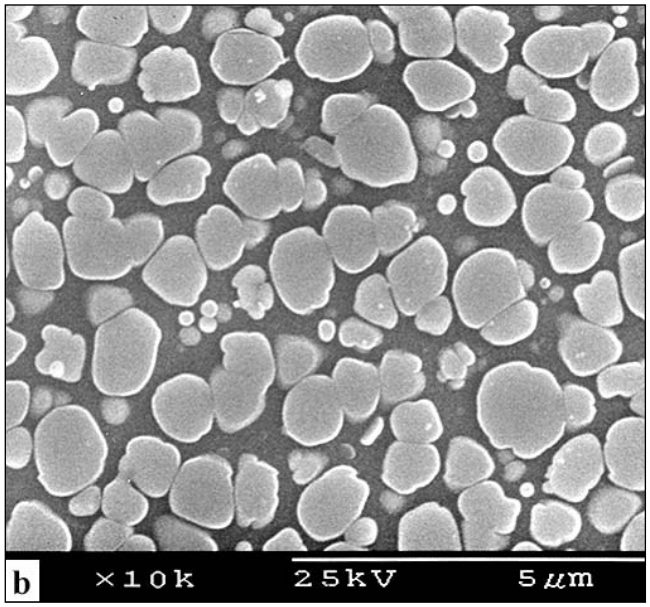


*Figure 4. Microstructure of the Blade 1 Leading Edge Specimen in the As-Received Condition. ((a) Optical micrograph; (b) SEM micrograph. Arrowheads indicate degenerated primary MC carbides. (Etchant–electrolytic chromic acid))*

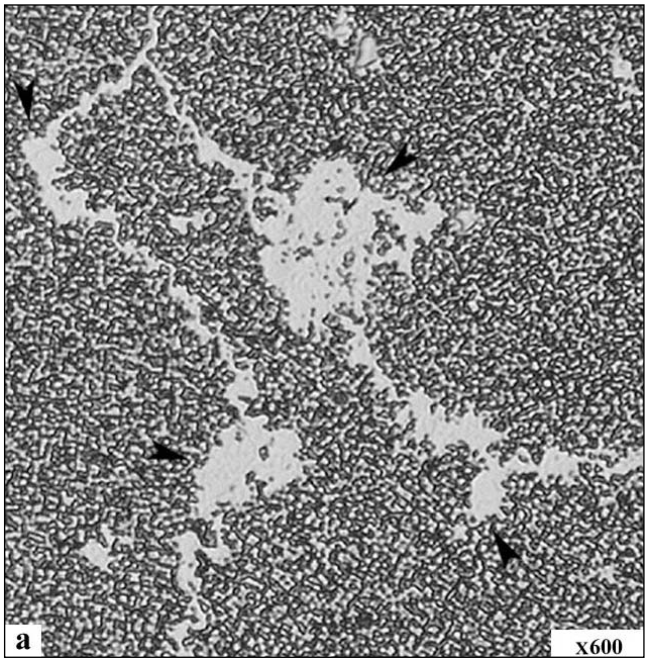


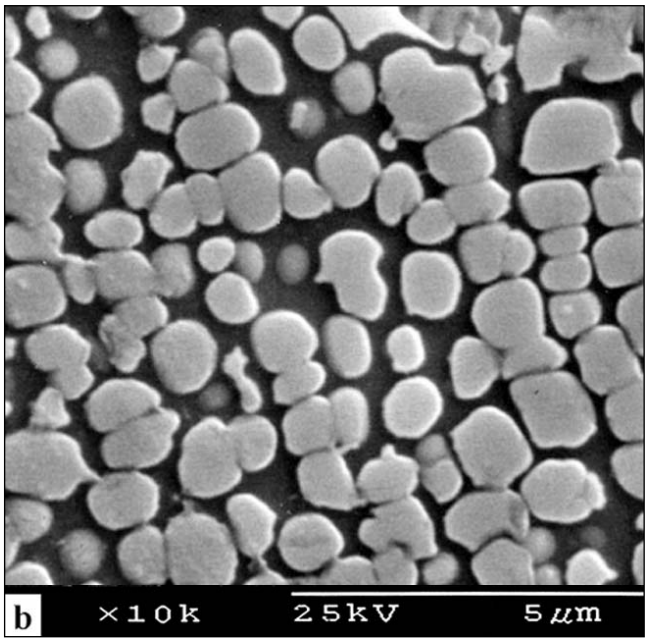


*Figure 5. Microstructure of the Blade 2 Leading Edge Specimen in the As-Received Condition. ((a) Optical micrograph; (b) SEM micrograph. Arrowheads indicate degenerated primary MC carbides. (Etchant–electrolytic chromic acid))*

The MC carbide decomposition reaction was reported to be $MC+\gamma \rightarrow M_{23}C_6 + \gamma'$ (Maccagno, et al., 1989; Ross and Sims, 1984; Castillo and Koul, 1986; Koul and Castillo, 1994). $M_{23}C_6$ carbides form at the periphery of the original MC carbides, and the area adjacent the MC core is supposed to consist of γ′-phase. The EDX spectra of the decomposition zone surrounding degenerated MC carbides in the service-exposed Blade 1 and Blade 2 leading edge specimens, given in Figures 6 and 7, did not confirm this assumption. These spectra demonstrate a presence of a substantial amount of carbon, which indicates that the phase from which they were taken cannot be γ′. The comparison of the spectrum from the γ′-particle with that from the MC decomposition zone in Figure 7 illustrates the difference.

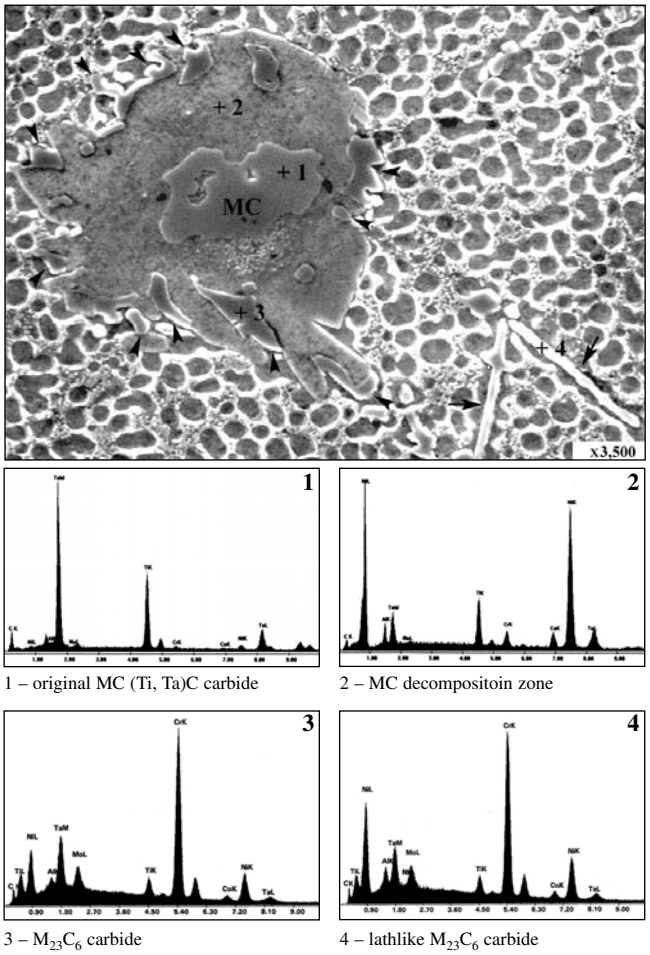


1 – original MC (Ti, Ta)C carbide

2 – MC decompositoin zone

3 – $M_{23}C_6$ carbide

4 – lathlike $M_{23}C_6$ carbide

*Figure 6. SEM Micrograph and EDX Spectra of the Degenerated MC Carbide in the Blade 1 Leading Edge Specimen in the As-Received Condition. ($M_{23}C_6$ carbides formed at the edges of the original MC carbide (arrowheads). $M_{23}C_6$ carbides precipitated also in the lathlike morphology (arrows). Energy-dispersive X-ray spectra from marked locations in the micrograph are shown. (Etchant–Kalling's reagent))*

The backscattered electron imaging (BEI) mode of SEM was used to study the microstructure of as-polished specimens because this method is capable of differentiating microstructural constituents based on their average atomic weight, without the interference of etching. The BEI micrographs and the results of EDS analysis of the degenerated MC carbides in GTD-111 and IN-738 alloys are presented in Figures 8 and 9. The BEI micrographs show a presence of dark $M_{23}C_6$ carbides at the MC periphery formed as discrete particles and as laths. A gradual change of the contrast of MC carbide toward its edges can be noted indicating a change of its chemical composition (it is known that the elemental concentration of MC carbides can vary in a wide range). There is a noticeable difference between γ′ contrast and that of the MC decomposition zone. If one of the products of the MC decomposition were γ′-phase, it would have had the same contrast as the original γ′-phase. This observation allows the conclusion that γ′-phase does not form during MC decomposition.

EDS analysis results show a substantial change of the MC carbide elemental concentration toward its edges; a tendency of carbon content to decrease from the center to the periphery is evident (Figures 8 and 9). Apparently, diffusion of carbon from the metastable MC carbide into the surrounding γ-matrix takes place during prolonged thermal exposure, creating a favorable condition for a formation of more stable lower-order $M_{23}C_6$ carbides on the MC/γ interface. The MC carbides serve as a carbon source and

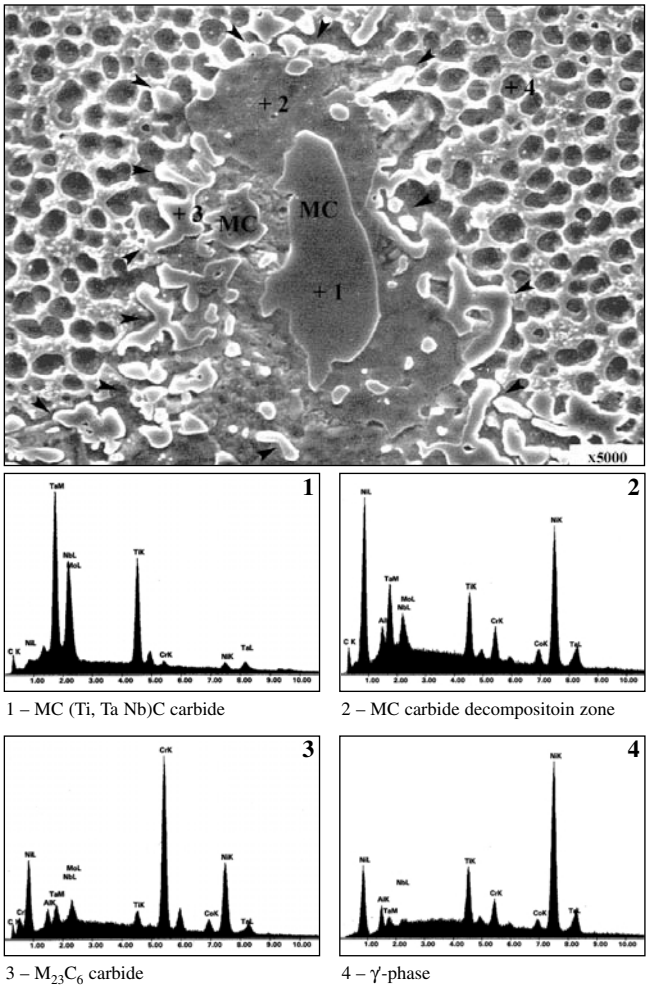


*Figure 7. SEM Micrograph and EDX Spectra of the Degenerated MC Carbide in the Blade 2 Leading Edge Specimen in the As-Received Condition. ($M_{23}C_6$ carbides formed at the edges of the original MC carbide (arrowheads). Arrowheads indicate $M_{23}C_6$ carbides formed at the edges of the original MC carbides as a result of MC decomposition. Energy-dispersive X-ray spectra from marked locations in the micrograph are shown. (Etchant–Kalling's reagent))*

γ-matrix as a chromium reservoir for a formation of chromium-rich $M_{23}C_6$ carbides. In light of these findings, the MC decomposition reaction can be informally presented as follows:

$$MC + \gamma \rightarrow M_{23}C_6 + (MC)_{deg} \quad (1)$$

where $(MC)_{deg}$ is a degenerated MC carbide with a reduced carbon content.

It should be noted that primary MC carbides located at or near the grain boundaries demonstrate easier decomposition than those in the grain interiors, and this fact is consistent with the abundance of the grain-boundary $M_{23}C_6$ precipitation. Evidently, the grain-boundary diffusion assists the process of the MC decomposition.

*The Blades after Rejuvenation*

The rejuvenation of four examined blades was successful in the restoration of the material's properties. Stress-rupture life of the mid-airfoil material has dramatically increased, as well as the alloy plasticity (Table 4). The stress-rupture test results were expressed in terms of the Larson-Miller parameter, which ties together temperature, stress, and time to fracture, and allows comparison of the results of tests conducted under different conditions.

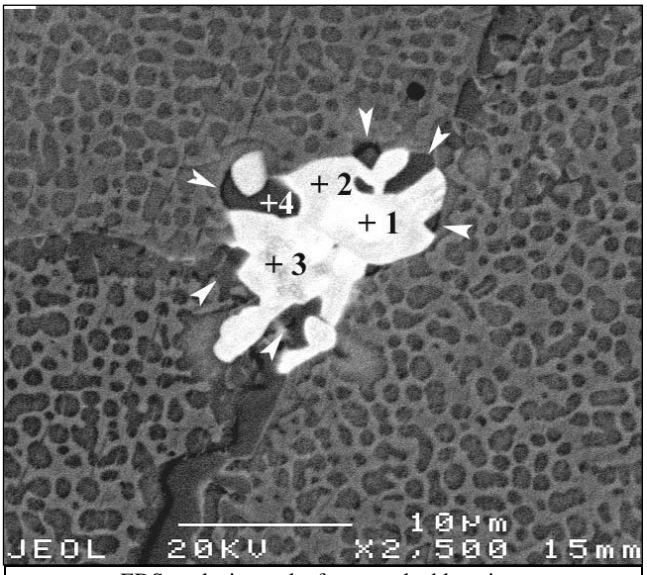


EDS analysis results from marked locations

| Location | Concentration, at. % | | | | | | | |
|---|---|---|---|---|---|---|---|---|
| | C | Al | Ti | Ta | Mo | Cr | Co | Ni |
| 1 | 55.7 | 1.3 | 17.5 | 15.6 | 0.7 | 0.6 | 0.8 | 7.78 |
| 2 | 14.2 | 7.1 | 15.5 | 7.4 | 0.6 | 1.7 | 4.5 | 49.0 |
| 3 | 13.4 | 6.9 | 10.2 | 8.5 | 0.5 | 1.4 | 5.0 | 54.1 |
| 4 | 35.2 | 0.2 | 1.5 | 1.8 | 2.4 | 47.1 | 1.8 | 10.0 |

*Figure 8. SEM-BEI Micrograph of the Degenerated MC Carbide in the Blade 1 Leading Edge Specimen in the As-Received Condition. ($M_{23}C_6$ carbides (arrowheads) formed at the periphery of original MC carbide as a result of the MC decomposition. EDS analysis data from marked locations are shown in the table. (As-polished))*

$$P = (460 + T)(20 + \log t) \quad (2)$$

where:
T = Test temperature, °F
t = Time to rupture, hr

The stress-rupture test results were compared to published data for new fully heat-treated alloys (*Aerospace Structural Metals Handbook*, 1997; *Heat-Resistant Materials*, 1997; *Atlas of Creep and Stress-Rupture Curves*, 1998). Larson-Miller parameter *P* for the rejuvenated airfoil is shown to fall within the scatter band for a new fully heat-treated material, which indicates complete stress-rupture properties restoration (Figure 10). The micro-hardness of the leading edge specimens after the rejuvenation has also increased significantly reaching the values of the shank (Table 5).

The improvement of the material properties was a result of the restoration of the airfoil microstructure. The micrographs in Figures 11 and 12 reveal the elimination of the excessive grain-boundary carbide precipitation, and the refinement of the primary and secondary γ' particles. The morphology of the primary γ' particles is cuboidal, with the average side size 0.6 μm in GTD-111 and 0.4 μm in IN-738. The microstructure of the rejuvenated leading edge specimens looks similar to that of the shank in the as-received condition, except for primary MC carbide morphology: instead of large blocky particles with sharp edges, there are fragments of the original primary carbides present (Figures 11a and 12a). The products of the MC carbide decomposition ($M_{23}C_6$ carbides and low-carbon degenerated portions of MC carbides) were dissolved in γ-solid solution during

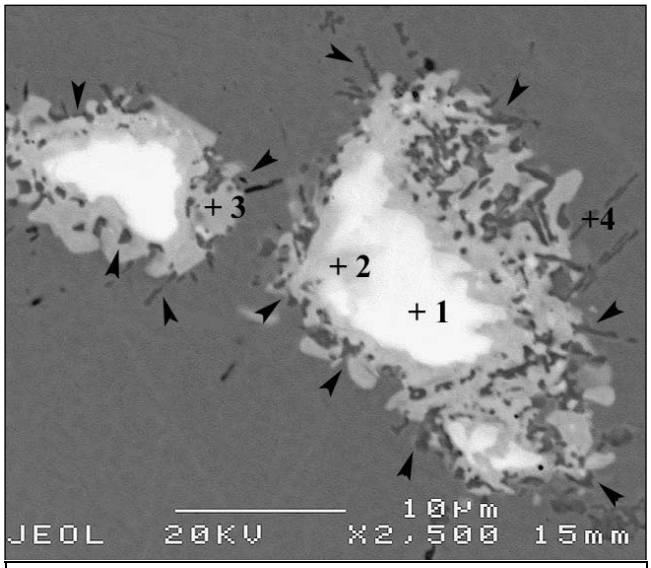


| EDS analysis results from marked locations | | | | | | | | | |
|---|---|---|---|---|---|---|---|---|---|
| Location | Concentration, at. % | | | | | | | | |
| | C | Al | Ti | Ta | Mo | Nb | Cr | Co | Ni |
| 1 | 47.4 | 0.97 | 18.5 | 12.3 | 3.24 | 8.96 | 2.48 | 1.21 | 4.94 |
| 2 | 26.7 | 4.31 | 6.86 | 9.19 | 1.36 | 3.83 | 6.21 | 3.14 | 38.4 |
| 3 | 23.1 | 2.70 | 5.91 | 3.69 | 0.97 | 3.61 | 12.9 | 5.02 | 42.1 |
| 4 | 18.9 | 2.24 | 2.11 | 1.24 | 2.51 | 0.80 | 37.4 | 5.7 | 29.1 |

*Figure 9. SEM-BEI Micrograph of the Degenerated MC Carbides in the Blade 2 Leading Edge Specimen in the As-Received Condition. ($M_{23}C_6$ carbides (arrowheads) formed at the periphery of original MC carbides as a result of the MC decomposition. EDS analysis data from marked locations are shown in the table. (As-polished))*

*Table 4. Stress-Rupture Test Results after Rejuvenation.*

| Specimen location | Blade 1 airfoil | Blade 2 airfoil | Blade 3 airfoil | Blade 4 airfoil |
|---|---|---|---|---|
| Test conditions | 1500ºF @ 70 ksi | 1500ºF @ 65 ksi | 1500ºF @ 65 ksi | 1500ºF @ 65 ksi |
| Time to fracture, hr | 130.9 | 94.1 | 89.6 | 114.9 |
| Elongation, % | 7.7 | 7.3 | 8.4 | 7.9 |
| Reduction in area, % | 14.6 | 12.3 | 12.2 | 11.9 |

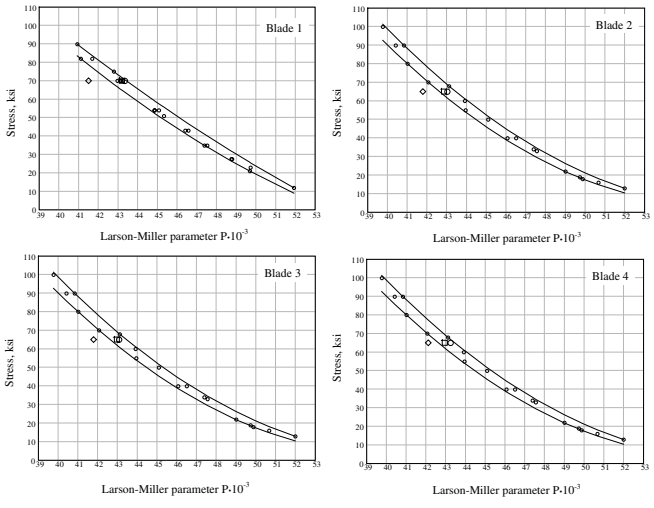


*Figure 10. Stress-Rupture Test Results in Terms of Larson-Miller Parameter. ((o) Published data for a new alloy; (▫) Shank as-received; (◇) Airfoil as-received; (O) Airfoil after rejuvenation.)*

*Table 5. Microhardness of the Blades after Rejuvenation.*

| MICROHARDNESS $H_V$ | | | | | | | |
|---|---|---|---|---|---|---|---|
| **Blade 1** | | **Blade 2** | | **Blade 3** | | **Blade 4** | |
| Shank | Leading edge | Shank | Leading edge | Shank | Leading edge | Shank | Leading edge |
| 431 | 430 | 429 | 432 | 414 | 416 | 406 | 404 |

HIP, leaving remnants of original primary MC carbides—an unaffected core surrounded with small MC fragments. The EDS analysis data in Figures 13 and 14 show lower carbon concentrations in the surrounding debris compared with that of the unaffected central part of the original MC carbides. Obviously, dissolved degenerated MC portions had even lower carbon concentration.

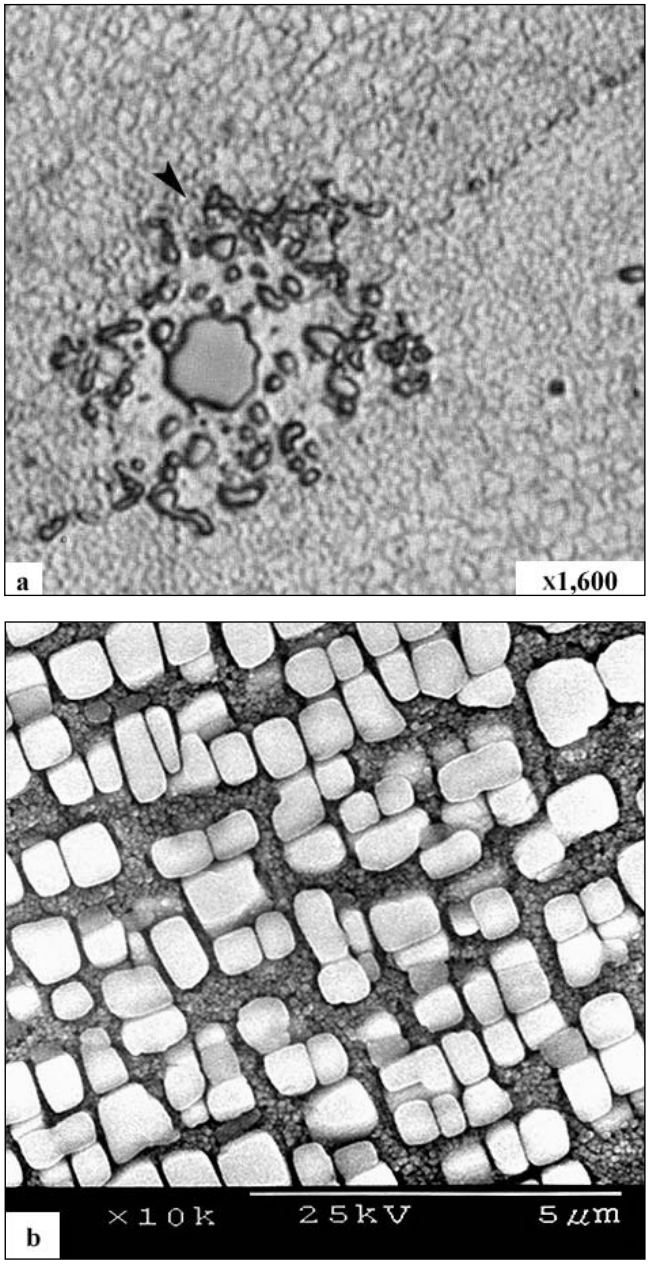


*Figure 11. Micrographs of the Blade 1 Leading Edge Specimen After Rejuvenation. ((a) Optical micrograph; (b) SEM micrograph. Arrowhead indicates disintegrated primary MC carbide. (Etchants: (a) Kalling's reagent; (b) Electrolytic chromic acid.))*

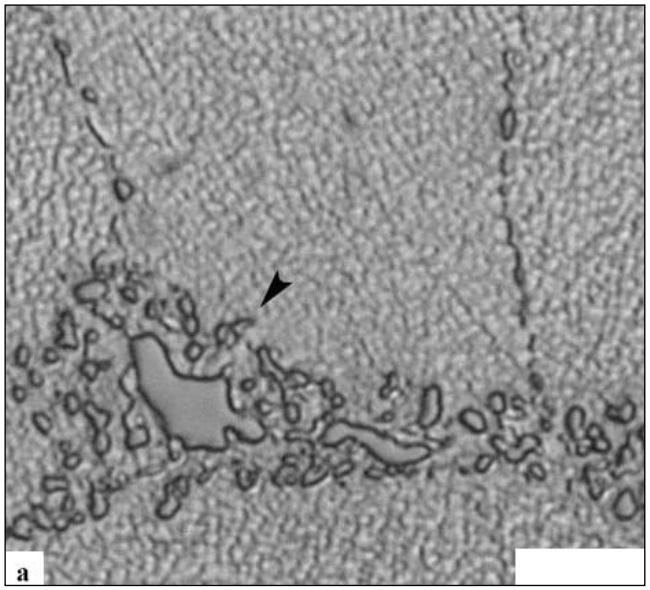


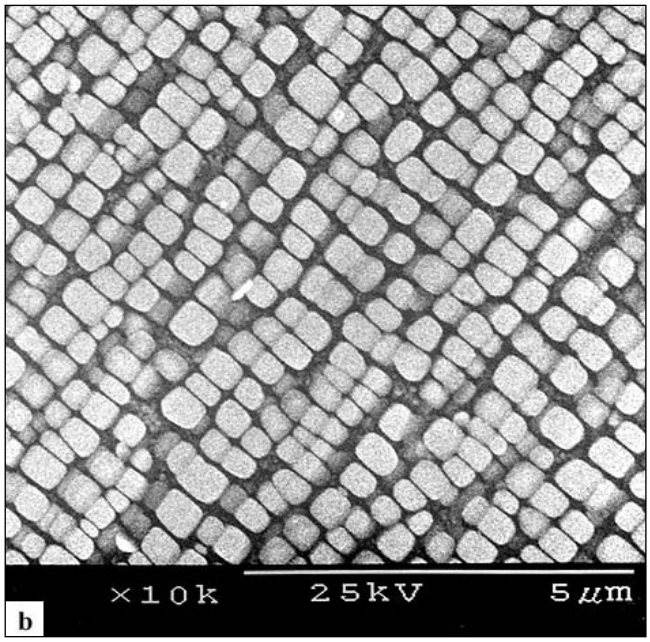


*Figure 12. Micrographs of the Blade 2 Leading Edge Specimen after Rejuvenation. ((a) Optical micrograph; (b) SEM micrograph. Arrowhead indicates disintegrated primary MC carbide. (Etchants: (a) Kalling's reagent; (b) Electrolytic chromic acid.))*

Dissolving of the degenerated portions of the primary MC carbides and a profusion of $M_{23}C_6$ carbides formed during the MC decomposition causes a release of additional amounts of carbon into the γ-solid solution, although overall carbon concentration is very low, and the difference between carbon concentration in the original γ-matrix and that in the rejuvenated alloy's γ-matrix could not be detected. An increased carbon concentration can affect the aging processes occurring in the superalloy and, furthermore, the behavior of the rejuvenated blades in the next service cycle. In order to verify this assumption, we studied the influence of 1000 hr aging at 1550°F on the microstructure, microhardness, and stress-rupture life of the rejuvenated blades.

*The Rejuvenated Blades after 1000 Hours Aging at 1550°F*

The effect of aging on the microstructure of the rejuvenated airfoils was compared to that of the shank, since the shank material

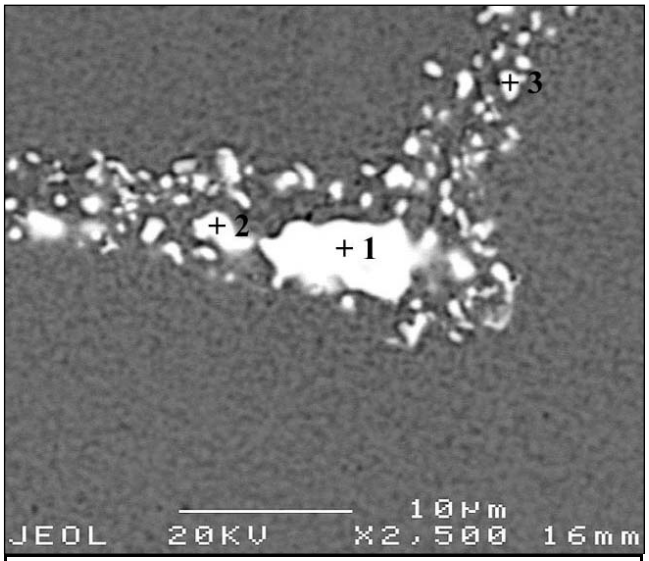


EDS analysis results from marked locations

| Location | Concentration, at. % | | | | | | | |
|---|---|---|---|---|---|---|---|---|
| | C | Al | Ti | Ta | Mo | Cr | Co | Ni |
| 1 | 50.65 | 2.92 | 24.05 | 15.65 | 0.8 | 1.1 | 1.98 | 2.85 |
| 2 | 27.67 | 5.95 | 12.78 | 9.86 | 2.45 | 8.09 | 2.95 | 30.25 |
| 3 | 20.94 | 5.65 | 3.55 | 1.92 | 0.25 | 13.07 | 8.25 | 46.37 |

*Figure 13. SEM-BEI Micrograph of the Degenerated MC Carbide in the Blade 1 Leading Edge Specimen after Rejuvenation. (EDS analysis results from marked locations are shown in the table. (As-polished))*

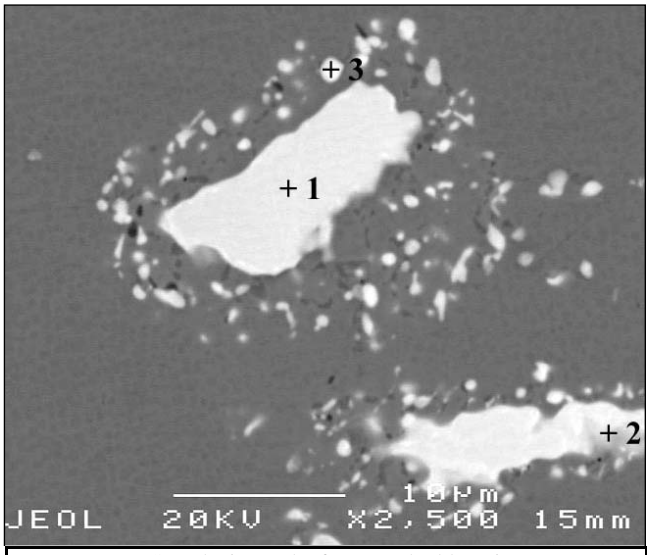


EDS analysis results from marked locations

| Location | Concentration, at. % | | | | | | | | |
|---|---|---|---|---|---|---|---|---|---|
| | C | Al | Ti | Ta | Mo | Nb | Cr | Co | Ni |
| 1 | 49.2 | 0.98 | 18.6 | 13.9 | 2.97 | 9.74 | 0.93 | 0.51 | 3.21 |
| 2 | 38.2 | 0.71 | 16.8 | 11.4 | 0.36 | 4.65 | 2.36 | 1.83 | 23.7 |
| 3 | 23.4 | 4.96 | 8.13 | 5.42 | 0.47 | 2.88 | 10.8 | 6.56 | 37.4 |

*Figure 14. SEM-BEI Micrograph of the Degenerated MC Carbides in the Blade 2 Leading Edge Specimen after Rejuvenation. (EDS analysis results from marked locations are shown in the table. (As-polished))*

showed no primary MC carbide decomposition during service. The micrographs of the rejuvenated shank and leading edge specimens after 1000 hr aging at 1550°F are presented in Figures 15, 16, 17, and 18; they reveal a significant acceleration of the aging process in the leading edge compared to the shank. While the microstructure of the rejuvenated Blade 1 shank is similar to that in the as-received condition (practically "as-new" material, Figure 15a), the Blade 1 leading edge microstructure demonstrates characteristic signs of overaging: excessive secondary carbide precipitation on the grain boundaries (Figure 16a) and γ′ coarsening (Figure 18a). The SEM backscattered electron image in Figure 16a shows a change of the contrast of the MC fragments, that is, a previously degenerated MC carbide readily decomposed during aging.

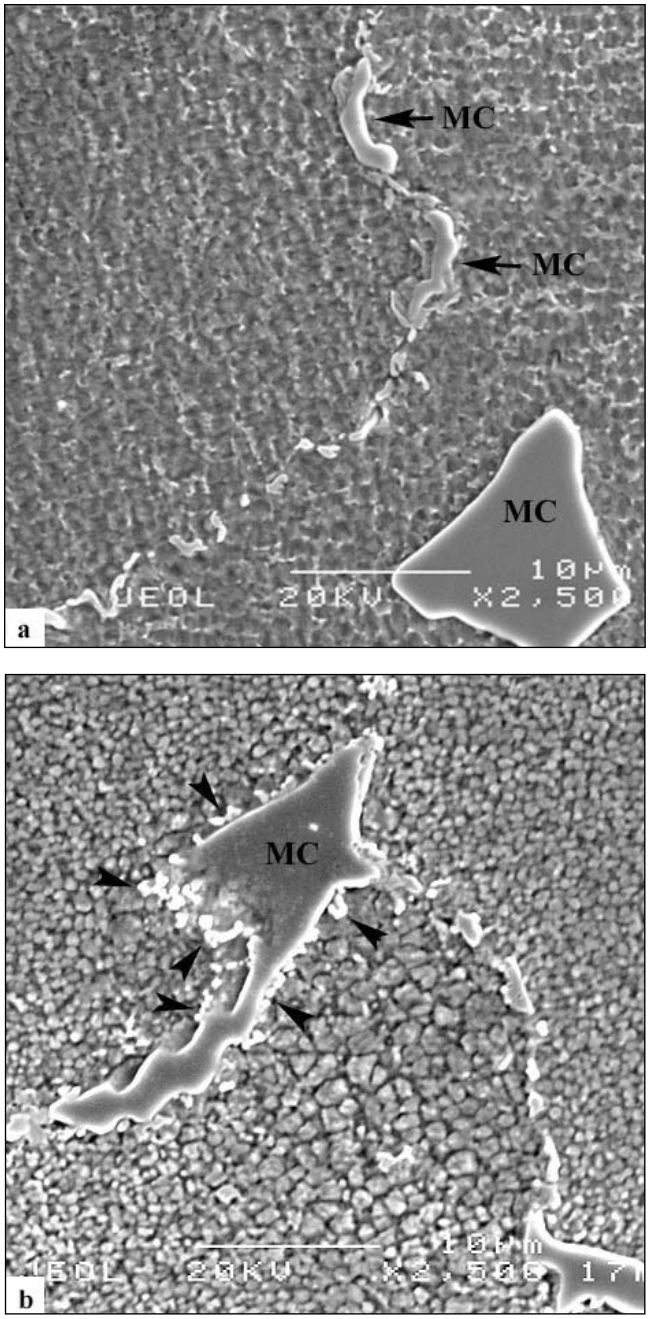


*Figure 15. SEM Micrographs of Rejuvenated Blade 1 (a) and Blade 2 (b) Shank Specimens after 1000 Hours Aging at 1550°F. (Arrowheads in (b) indicate fine $M_{23}C_6$ precipitates at MC carbide edges. (a) BEI (as-polished); (b) SEI. (Etchant–Kalling's reagent))*

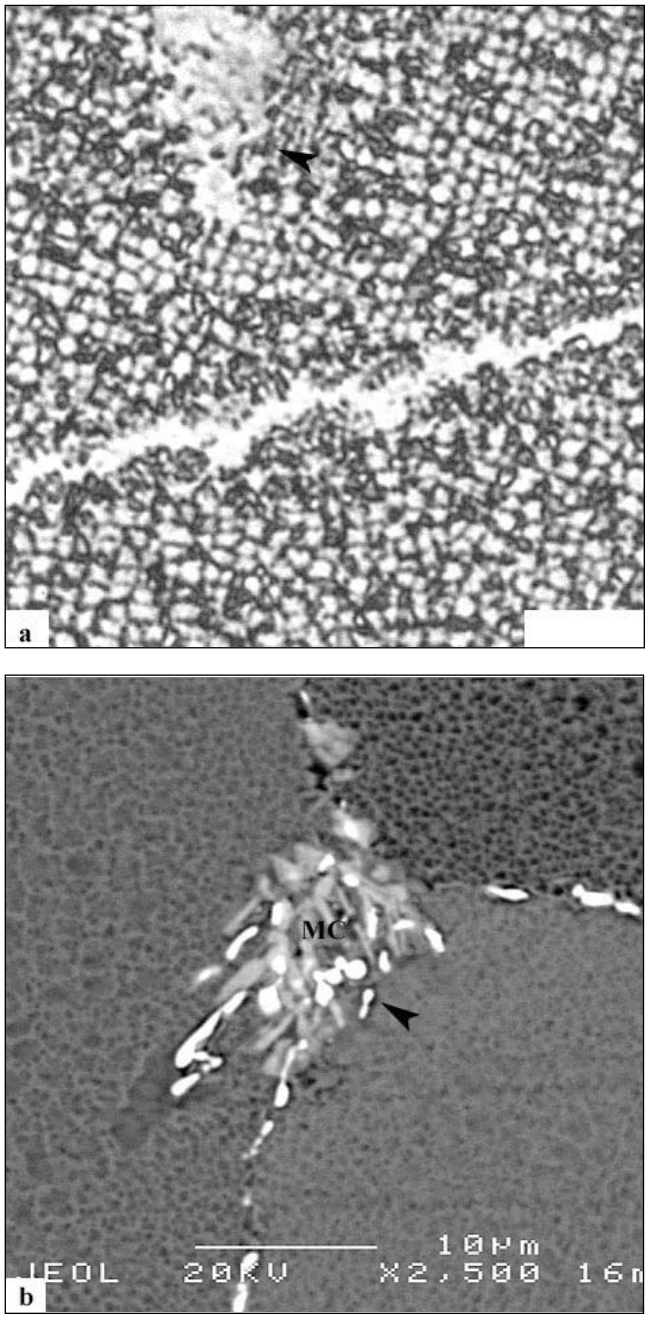


*Figure 16. Micrographs of Rejuvenated Blade 1 Leading Edge Specimen after 1000 Hours Aging at 1550°F. (Arrowheads indicate previously degenerated MC carbide continuing to deteriorate during aging. (a) Optical micrograph (etchant, electrolytic chromic acid); (b) SEM-BEI micrograph (as-polished).)*

The comparison of the rejuvenated Blade 2 shank and leading edge microstructures after aging demonstrates a similar tendency, although the aged shank specimen reveals a presence of early stages of the MC decomposition: the SEM secondary electron image in Figure 15b shows a number of very fine globular $M_{23}C_6$ carbides formed around primary MC carbides. The microstructure of the rejuvenated and aged Blade 2 leading edge is typically overaged, with the grain boundaries overloaded by $M_{23}C_6$ carbides (Figure 17a) and coarsened and coalesced γ′ (Figure 18b). The SEM backscattered electron micrograph in Figure 17b shows gradually changing MC carbide contrast due to additional decomposition of the previously degenerated MC carbides.

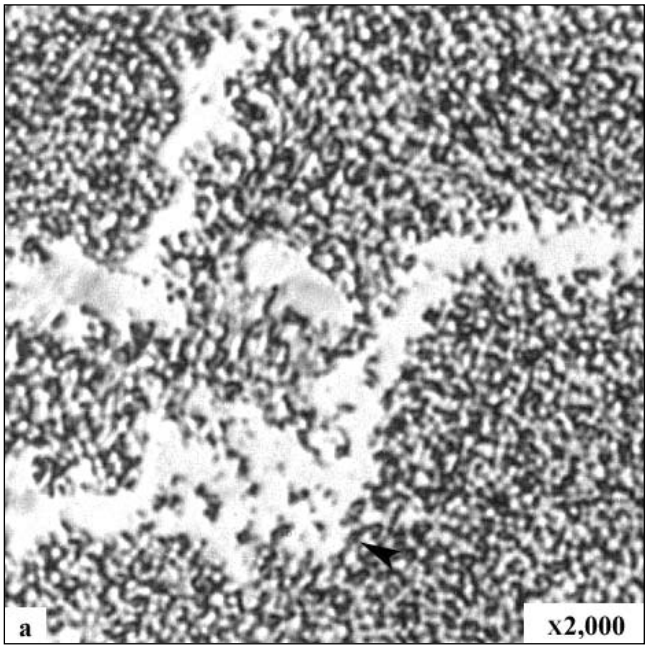


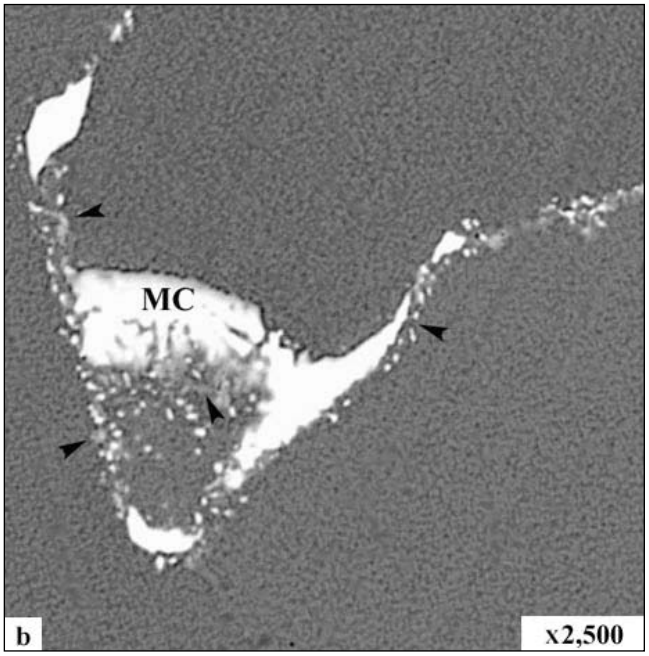


*Figure 17. Micrographs of Rejuvenated Blade 2 Leading Edge Specimen after 1000 Hours Aging at 1550°F. (Arrowheads indicate previously degenerated MC carbide continuing to deteriorate during aging. (a) Optical micrograph (etchant, electrolytic chromic acid); (b) SEM-BEI micrograph (as-polished).)*

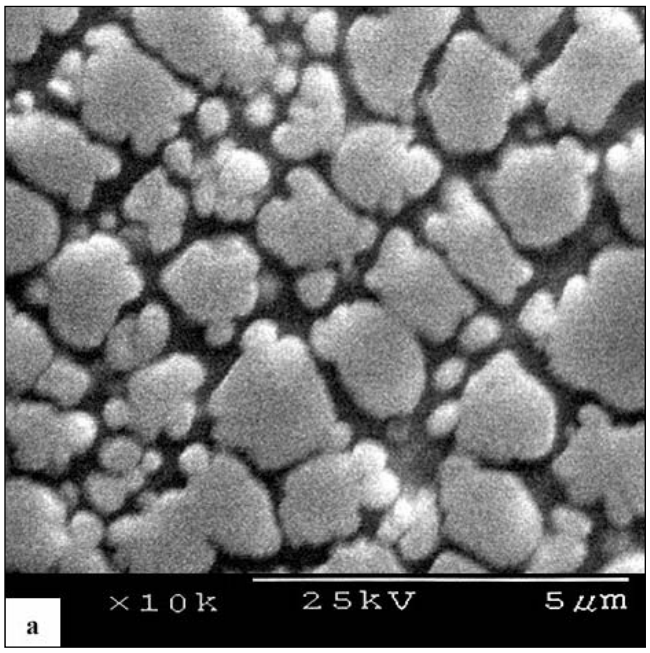


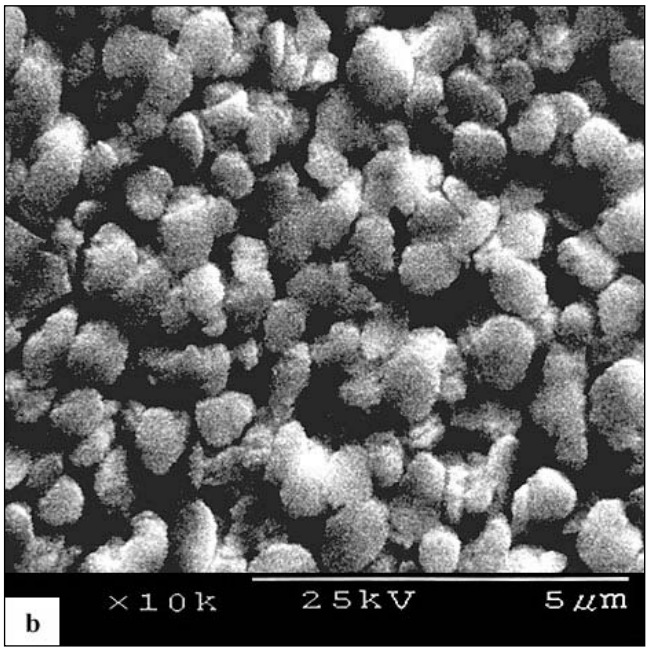


*Figure 18. SEM Micrographs of Rejuvenated Blade 1 (a) and Blade 2 (b) Leading Edge Specimens after 1000 Hours Aging at 1550°F. (Etchant–electrolytic chromic acid)*

The difference in the microstructure of the rejuvenated and aged shank and leading edge specimens is reflected in their microhardness: while the shank microhardness decreases slightly, the reduction of the leading edge microhardness is substantial (Figure 19). The results of the short-term stress-rupture tests also display the difference between rejuvenated and aged shank and mid-airfoil behavior. The acceleration of the aging process in the rejuvenated airfoil caused a noticeable reduction of its stress-rupture life and plasticity compared to that of the shank (Figure 20). A comparison of the SEM micrographs of the shank and airfoil fracture surfaces illustrates the difference of the fracture mode (Figure 21). The shank specimen from the rejuvenated and aged Blade 4 demonstrates predominantly transgranular ductile fracture (Figure 21a, b), while the fracture surface of the mid-airfoil specimen shows distinct interdendritic-intergranular fracture with a formation of the grain-boundary cavities caused by a heavy secondary carbide precipitation (Figure 21c, d).

The results of the aging experiment demonstrate an obvious effect of the advanced service-induced primary MC carbide decomposition on the aging rate of rejuvenated gas turbine blades. The aging process has evidently accelerated in the mid-airfoil in comparison with the shank resulting in more rapid excessive secondary $M_{23}C_6$ carbides formation on the grain boundaries, which is detrimental to creep resistance and reduces alloy ductility. The cause of it appears to be the release of additional amounts of carbon into γ-solid solution from dissolving of the MC carbide

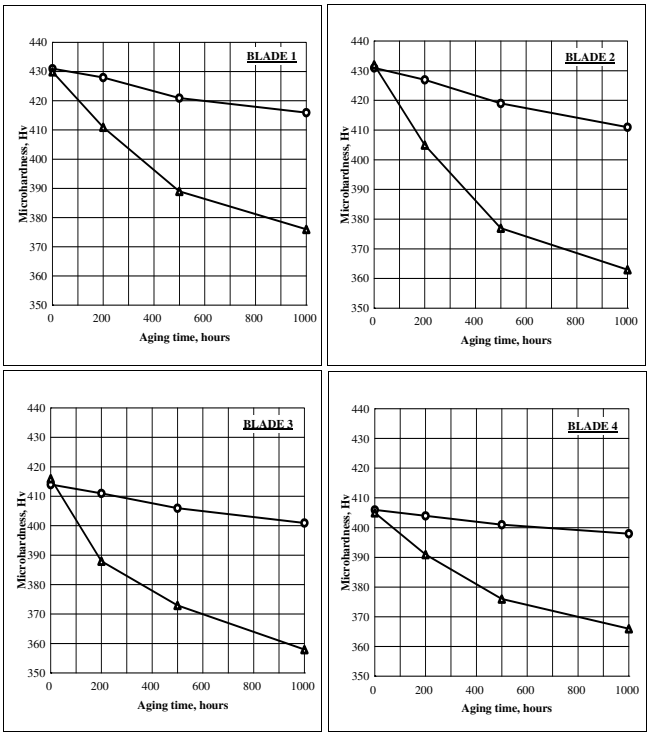


*Figure 19. Influence of Aging at 1550°F on the Microhardness of Rejuvenated Blades. ((O) Shank; (Δ) Leading edge.)*

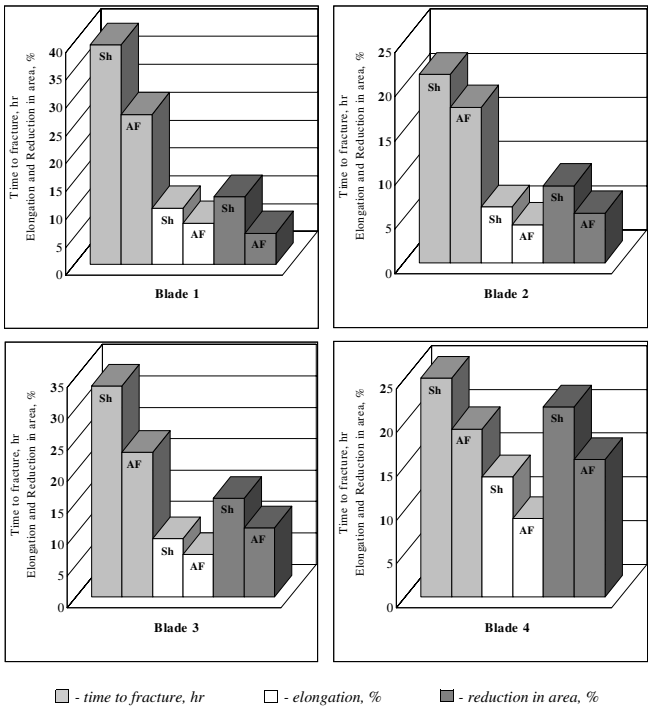


*Figure 20. Results of Short-Term Stress-Rupture Test of the Rejuvenated Blades after 1000 Hours Aging at 1550°F. ((R) Shank specimens; (AF) Airfoil specimens.*

decomposition products during rejuvenating HIP or solution annealing. The aging acceleration can be expected to be higher when service-induced microstructural deterioration is more advanced, as happens often in the modern machines with the firing temperatures above 2300°F, despite the use of protective coatings and internal cooling. In order to extend the blade's life it seems to

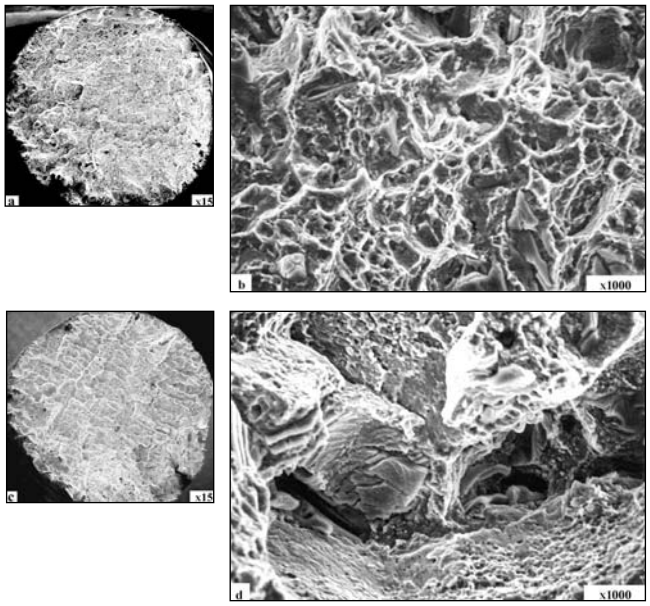


*Figure 21. SEM Micrographs of the Fracture Surfaces of Rejuvenated and Aged Blade 4 Stress-Rupture Test Specimens. ((a, b) Shank specimen; (c, d) Airfoil specimen. Arrowheads indicate grain-boundary cavities (d).)*

be prudent to avoid the extensive primary MC carbide decomposition by reducing the periods between rejuvenations, in order to prevent the advanced development of this process. More frequent rejuvenations will prolong blade life and, despite the extra cost of additional rejuvenations, will save money on the blade replacement in the long run.

## CONCLUSIONS

• The detailed study of the service-induced primary MC carbide decomposition processes in the GTD-111 and IN-738 gas turbine blades has been conducted. It was found that MC decomposition during thermal exposure follows the reaction shown in Equation (1).

• Service-induced primary MC carbide decomposition is irreversible, and was shown in this study to have a significant effect on the aging kinetics of rejuvenated material. An advanced primary MC carbide degeneration leads to increasing carbon and carbide-forming element concentration in the γ-solid solution during rejuvenation due to dissolving of the MC carbide decomposition products. This process results in the γ-matrix chemistry changes, which, in turn, affect the alloy properties in the next service cycle:

- Secondary $M_{23}C_6$ carbides precipitate more rapidly on the grain boundaries, reducing the alloy's ductility and creep strength.
- Strengthening elements, such as Cr and Mo, leave the γ-matrix more rapidly, forming abundant secondary carbides, thus reducing its strength at a greater rate compared with a new alloy.
- Coarsening and coalescence of γ′-phase occurs more rapidly, reducing the creep resistance.

• The detrimental effect of the MC decomposition can be minimized by reducing the periods between rejuvenations in order to prevent the advanced development of this process. This will accomplish the following:

- Minimize the operational time when the alloy properties are reduced, thereby minimizing the risk of creep damage.
- Minimize the risk of cracks, erosion, and other surface degradation due to extended operation with damaged coating.

• The subject of this study is very complex and requires further investigation in order to better understand the processes occurring in the rejuvenated gas turbine blades. The study continues in the Metallurgical Laboratory at the authors' company.

## REFERENCES

*Aerospace Structural Metals Handbook*, 1997, *5*, CINDAS/USAF CRDA Handbooks Operation, Purdue University.

ASTM E139, 1996, "Standard Test Methods for Conducting Creep, Creep-Rupture, and Stress-Rupture Tests of Metallic Materials," American Society for Testing and Materials, West Conshohocken, Pennsylvania.

*Atlas of Creep and Stress-Rupture Curves*, 1998, Materials Park, Ohio: ASM International Publications.

Baldan, A., 1995, "Extension of the Creep Life of a Conventionally Cast Nickel-Base Superalloy by Regenerative Heat Treatment," Proceedings of the Conference on Materials Aging and Component Life Extension, *II*, Milan, Italy, Engineering Materials Advisory Services Ltd., United Kingdom, pp. 943-950.

Beddoes, J. C. and Walace, W., 1980, "Heat Treatment of Hot Isostatically Processed IN-738 Investment Castings," *Metallography*, *13*, pp. 185-194.

Castillo, R. and Koul, A. K., 1986, "Effects of Microstructural Instability on the Creep and Fracture Behavior of Cast IN-738lC Ni-Base Superalloy," Proceedings of the Conference on High Temperature Alloys for Gas Turbines and other Applications, Liege, Belgium, pp. 1395-1410.

Daleo, J. A. and Wilson, J. R., 1998, "GTD111 Alloy Material Study," Journal of Engineering for Gas Turbines and Power, *120*, ASME Paper 96-GT-520.

Floyd, P. H., Wallace, W., and Immarigeon, J. P. A., 1983, "Rejuvenation of Properties in Turbine Engine Hot Section Components by Hot Isostatic Pressing," Proceedings of the Conference on Heat Treatment '81, Birmingham, England, The Metal Society, pp. 97-102.

Hakl, J., Bina, V., Kudrman, J., and Pech, R., 1995, "Blade Life Prolongation in Land Based Gas Turbines," Proceedings of the Conference on Materials Aging and Component Life Extension, *II*, Milan, Italy, Engineering Materials Advisory Services Ltd., United Kingdom, pp. 991-1000.

*Heat-Resistant Materials*, 1997, Materials Park, Ohio: ASM International Publications.

Koul, A. K. and Castillo, R., 1988, "Assessment of Service-Induced Microstructural Damage and its Rejuvenation in Turbine Blades," Metallurgical Transactions A, *19A*, pp. 2049-2066.

Koul, A. K. and Castillo, R., 1994, "Creep Behavior of Industrial Turbine Blade Material," Proceedings of ASM 1993 Materials Congress, Pittsburgh, Pennsylvania, ASM International Publications, pp.75-88.

Maccagno, T. M., Koul, A. K., Immarigeon, J. P. A, Cutler, L., Allem, R., and L'Esperance, G., 1989, "Rejuvenation of Service Exposed Alloy 713C Turbine Blades," Report of National Aeronautical Establishment, National Research Council, Canada.

Ross, E. W. and Sims, C. T., 1984, *Superalloys II*, C. T. Sims, N. S. Stoloff, and W. C.Hagel, Editors, New York, New York: John Wiley & Sons, pp. 112-116.

Stevens, R. A. and Flewitt, P. E. J., 1978, "Microstructural Changes Which Occur During Isochronal Heat Treatment of the Nickel-Base Superalloy IN-738," Journal of Materials Science, *13*, pp. 367-376.

Stevens, R. A. and Flewitt, P. E. J., 1979a, "The Effect of γ'-Precipitate Coarsening During Isothermal Aging and Creep of the Nickel-Base Superalloy IN-738," Materials Science and Engineering, *37*, pp. 237-247.

Stevens, R. A. and Flewitt, P. E. J., 1979b, "Regenerative Heat Treatments for the Extension of the Creep Life of the Superalloy IN-738," *Strength of the Metals and Alloys*, *1*, Fifth International Conference, Aahen, West Germany, Pergamon Press, pp. 439-444.

Tawancy, H. M., Abbas, N. M., Al-Mana, A. I., and Rhys-Jones, T. N., 1994, "Thermal Stability of the Advanced Ni-Base Superalloys," Journal of Material Science, *29*, pp. 2445-2458.

Xuebing, H., Yan, K., Huihua, Z., Yun, Z., and Zhuiangqi, H., 1998, "Influence of the Heat Treatment on the Microstructure of a Unidirectional Ni-Base Superalloy," Materials Letters, *36*, pp. 210-213.

## ACKNOWLEDGEMENT

The authors wish to thank Dr. V. Levit and Dr. R. Crooks of the Black Laboratories, L.L.C., for valuable discussions during the course of this work.